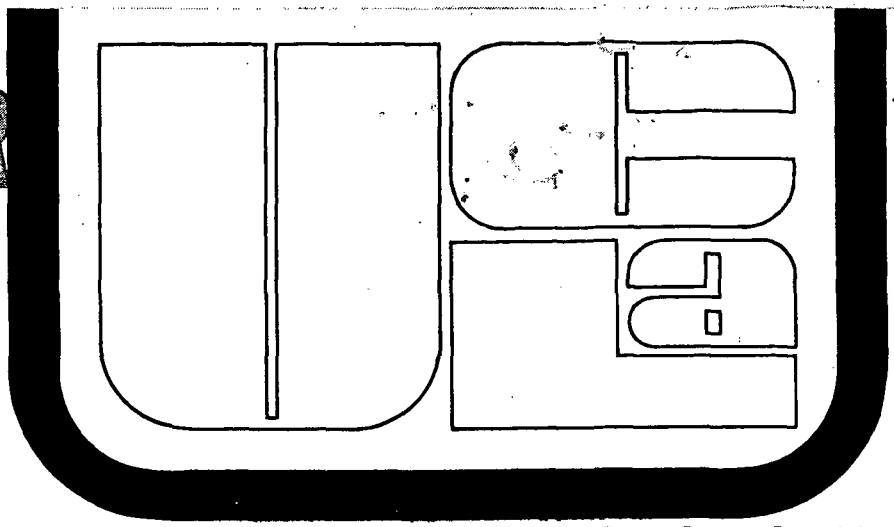

PLASMA PHYSICS GROUP

Turbulent Resistivity, Diffusion and Heating

Burton D. Fried, Charles F. Kennel, Kenneth MacKenzie
Ferdinand V. Coroniti, Joseph M. Kindel, R. Stenzel,
Robert J. Taylor, Roscoe White, Alfred Y. Wong,
William Bernstein, J. M. Sellen, Jr.,
David Forslund and R. Z. Sagdeev

June, 1971 R-9

UNIVERSITY OF CALIFORNIA
LOS ANGELES

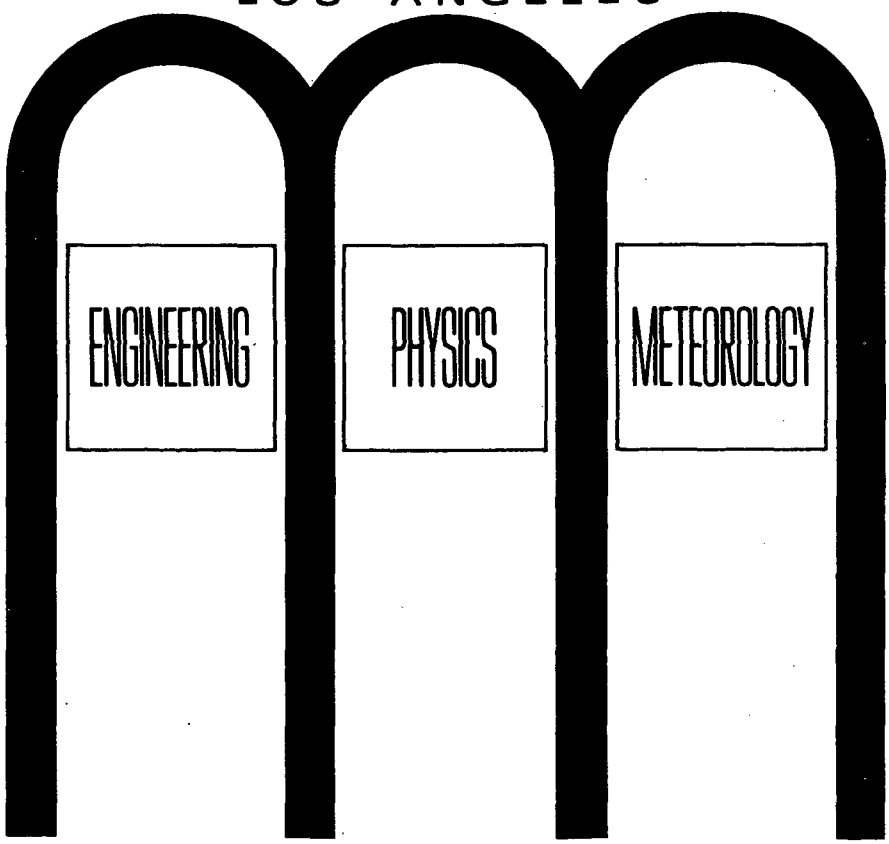

Turbulent Resistivity, Diffusion and Heating

Burton D. Fried, Charles F. Kennel, Kenneth MacKenzie,
Ferdinand V. Coroniti, Joseph M. Kindel, R. Stenzel,
Robert J. Taylor, Roscoe White, Alfred Y. Wong,
William Bernstein, J. M. Sellen, Jr.,
David Forslund and R. Z. Sagdeev

June, 1971 R-92

Plasma Physics Group
Department of Physics
University of California
Los Angeles, California 90024

TURBULENT RESISTIVITY, DIFFUSION AND HEATING* CN-28/E-4

BURTON D. FRIED†, CHARLES F. KENNEL†, KENNETH MACKENZIE, FERDINAND V. CORONITI, JOSEPH M. KINDEL††, R. STENZEL, ROBERT J. TAYLOR, ROSCOE WHITE and ALFRED Y. WONG
University of California, Los Angeles; WILLIAM BERNSTEIN and J. M. SELLEN, JR., TRW Systems; DAVID FORSLUND, Los Alamos Scientific Laboratory; and R. Z. SAGDEEV, Institute of High Temperatures, Moscow

ABSTRACT

Current flow with density $j > nec_s$ ($c_s \equiv \sqrt{T_e/m_i}$ = ion acoustic velocity) should encounter resistance due to ion acoustic turbulence when $T_e >> T_i$. This has been observed in experiments with a streaming cesium plasma ($B = 0$), in which electron current, potential rise due to turbulent resistivity, spectrum of unstable ion acoustic waves, and associated electron heating were all measured directly. Kinetic theory calculations for an expanding, unstable plasma, give results in agreement with experiment. The effective electron collision frequency is of order 5 to 10 ω_{pi}. In a strong magnetic field, with $T_e/T_i \sim 1$ and current densities less than nea_e ($a_e = \sqrt{2T_e/m_e}$), typical for present Tokomaks, the plasma is stable to ion acoustic but unstable to current driven electrostatic ion cyclotron waves. Relevant characteristics of these waves are calculated and it is shown that for ion $\beta > m_e/m_i$, the electromagnetic ion cyclotron wave has a lower instability threshold than the electrostatic one. However, when ion acoustic turbulence is present ($T_e/T_i > 5$) experiments with Double Plasma (DP) devices show rapid anomalous heating of an ion beam streaming through a plasma. These DP devices also produce large amplitude, collisionless ion acoustic shocks, both laminar and turbulent. At low Mach numbers, a beam of reflected ions is observed. Turbulence, either natural or triggered by fluctuations of injected ion waves, scatters the reflected ions and heats the shocked ions (observed broadening of distribution function). Shock structure is very sensitive to T_e/T_i and especially to the presence of light ions: a few per cent He in an A plasma can significantly change both the shock amplitude and the laminar/turbulent transition. At higher density ratios (obtained with photoionization and microwave, upper hybrid, resonant heating) the Mach number increases (maximum observed ~ 1.8) and the structure washes out.

† Also at TRW Systems

†† Current address: Princeton Plasma Physics Laboratory

* This work was partially supported by the AEC, ONR, NASA, AFOSR, NSF and TRW Independent Research Program.

1. Introduction

We report here four related experimental and theoretical studies of ion acoustic and ion cyclotron turbulence and the role they play in anomalous resistivity, viscosity, diffusion and heating and in the structure of collisionless electrostatic shocks.

2. Anomalous Resistivity Due to Ion Acoustic Turbulence.

Experiments have been carried out on a quiescent, streaming, inertially confined cesium plasma with $T_e/T_i >> 1$ and no external magnetic field. The general configuration and dimensions are shown in Fig. 1 with the plasma

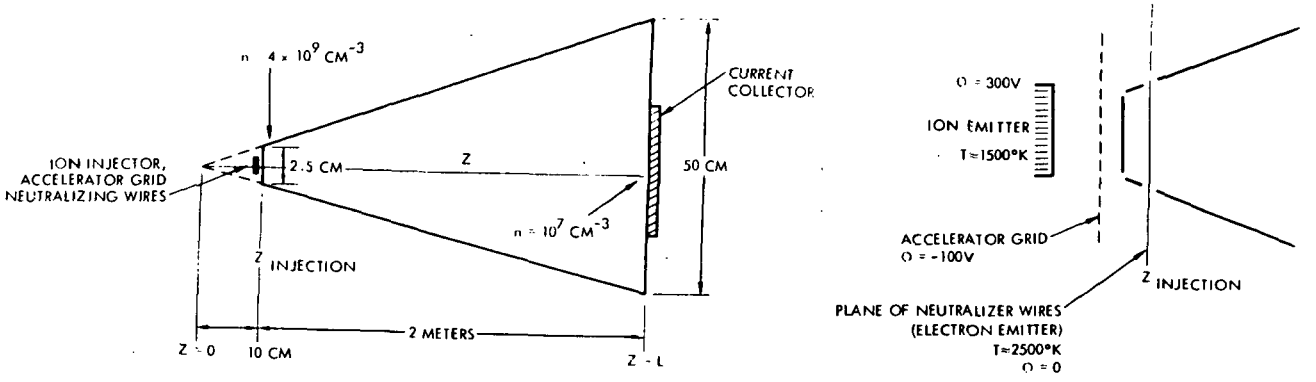

Fig. 1. Cesium ion beam configuration (on left) and enlarged view of plasma source (on right).

source [1] shown schematically on the right of Fig. 1. The collector electrode, 2 m from the source, may "float", drawing electron and ion currents, I_0, of order 6 mA; or it may be biased positively, resulting in an electron current flow, I, from neutralizer wires to collector electrode, $I_0 \leq I \lesssim 10\ I_0$. For $I = I_0$, the plasma potential on axis (measured with emissive probes) is nearly constant ($dV/dz \sim 10^{-2} - 10^{-3}$ V/cm) but as I is increased, a sharp rise in potential is observed (Fig. 2), at values of z

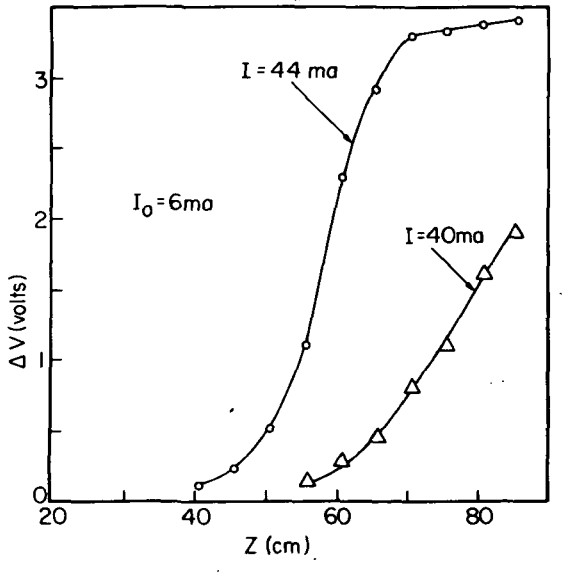

Fig. 2. Anomalous potential rise due to electron current flow.

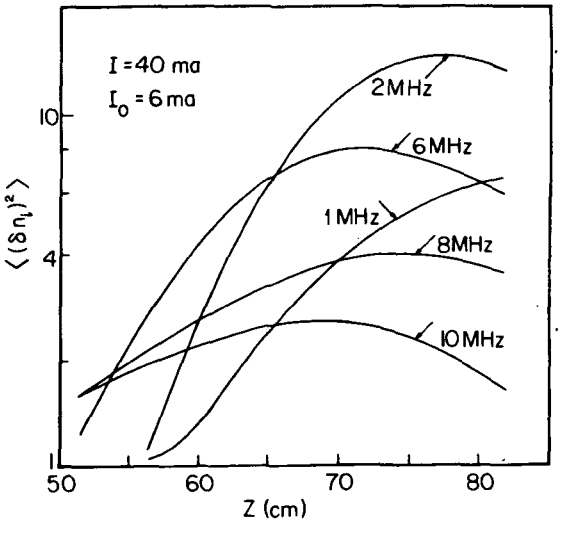

Fig. 3. Amplitude of ion acoustic noise (in arbitrary units) measured by Faraday cup.

which decrease with increasing I. Faraday cup measurement of ion acoustic noise show an abrupt rise in the same region (Fig. 3) and Langmuir probes show a correlated increase in electron temperature from the initial 0.25 eV to values comparable to ΔV. Growth of ion acoustic waves launched at the accelerating grid is also clearly observable when $I > I_0$.

Our theoretical analysis assumes, in conformity with experimental measurements, that plasma density (measured with Faraday cups) and current density (measured with small flux coils) are uniform inside a cone, $r = (r_0/z_0)z$, ($z_0 \simeq 10$ cm) so an observer moving with the ion streaming velocity, $v_0 \simeq 2\times10^6$ cm/sec, sees a density decreasing with time. Because $v_0 >> c_s = (T_e/M)^{1/2} \simeq 6\times10^4$ cm/sec, there is little propagation from one plasma region to another during the beam transit time and an initial-value formulation in the ion rest frame is appropriate, with lab frame frequency coming essentially from Doppler shift $\omega = k_z(v_0 \pm c_s) \simeq k_z v_0$. Linear theory predicts a wave growth from z_0 to z given by

$$\log\,[\delta E_k(z)/E_k(z_0)] = 2\int_{z_0}^{z} \mathrm{Im}\,\omega_k\, dz/V_0 = (\alpha/2)(k_z/k)\, h(\kappa,y) \qquad (1)$$

where $\delta E_k(z_0)$ is the fluctuation electric field at injection; $\kappa = k/k_D(z_0)$; $y = z/z_0$; $\alpha = (I/I_0)(\pi m/2M)^{1/2}\, k_D(z_0) \simeq 10\text{–}15$; $k_D(z_0) = (4\pi n(z_0)e/T_e)^{1/2}$;

$$h(\kappa,y) = \kappa y[1 + \kappa^2 y^2]^{-1/2} - (1 + \kappa^2)^{-1/2} \qquad (2)$$

In the anomalous resistivity region, the experimentally observed growth of ion acoustic turbulence (Fig. 2) agrees with Eq. (1) for the wave numbers of maximum growth [$\kappa \simeq K \equiv y^{2/3}\,(1 + y^{2/3})^{-1/2}$] but smaller wave numbers grow faster than predicted by Eq. (1), suggesting the presence of strong mode coupling as observed in other ion-acoustic wave experiments [2]. The electron velocity diffusion coefficient associated with this turbulence, calculated in the usual way [3] from the second order Vlasov equation, causes an anomalous viscosity for the electrons. In our constant current configuration, this must be overcome by a potential rise ΔV (Fig. 2). If $\tilde{E}$ is the associated electric field, the effective collision frequency, defined by $\tilde{\nu} = eE/mV_D$, is given by

$$\tilde{\nu}(z)/\omega_{pi}(z_0) = (M/m)^{1/2}\, G(y)/N_D(z_0) \qquad (3)$$

where $v_D = (I/I_0 - 1)v_0$; $N_D(z) = n(z)/K_D^3(z)$; and

$$G(y) = K^{5/2}(1 + K^2)^{-3/4}\, e^{\alpha H}/16\pi\sqrt{3}\alpha^{3/2} H(y^2 - y^{2/3}) \qquad (4)$$

with $H = h(K,y)$. Typical values of $\tilde{\nu}(z)/\omega_{pi}(z) = \tilde{\nu}(z)/y\omega_{pi}(z_0)$ are 5 to 10. In deriving (4), we use a saddle point approximation valid for large y and neglect variations in T_e. We also take $\langle|\delta E_k(z_0)|^2\rangle$ to correspond to bare particle discreteness, since the plasma transit time ($\sim$ 100 μs) is too short for formation of Debye shielding clouds. The early portions of the curves in Fig. 2 are in qualitative agreement with (3), but the experimental curves rise more rapidly with z, probably due to the aforementioned mode coupling. The calculated electron heating is also in agreement with the experimental values. In addition, it causes an enhanced beam divergence which appears to be the principal cause of the saturation of the anomalous potential rise in Fig. 2.

3. The Ion Cyclotron Instability

We report four basic extensions of the Drummond-Rosenbluth [4] investigation of the electrostatic ion cyclotron instability: arbitrary T_e/T_i = electron-to-ion temperature ratio; growth rates well above marginal stability; finite β_i corrections, where β_i is the ratio of ion particle to magnetic field pressure; and a comparison of the electrostatic and electromagnetic ion cyclotron current instabilities [20].

3.1 Electrostatic Ion Cyclotron Instabilities.

We have chosen isotropic Maxwellian distributions drifting along a uniform-background magnetic field. When $T_e/T_i = 1$, the wave that is marginally stable to the smallest current has $k_\perp^2 R_i^2 \simeq 1$, $\omega \simeq 1.2\Omega_{ci}$, and $k_\perp/k_\parallel = 12$, where R_i is the thermal ion Larmor radius, ω is the wave frequency and $k_\perp$, $k_\parallel$ are wave numbers perpendicular and parallel to B_0 [5], [6], [7]. Here we focus on unstable ion cyclotron waves. The dispersion relation [4], [5] depends upon $k_\perp^2 R_i^2$, $k_\perp/k_\parallel$, V_D/a_e [the electron drift relative ions in units $(2T_e/m_e)^{1/2}$], m/M, T_e/T_i, and the ratio of ion plasma to cyclotron frequency, $\omega_{pi}^2/\Omega_{ci}^2$. We eliminate some dependences: we take $\omega_{pi}/\Omega_{ci} > 10$, since this implies weak $\omega_{pi}^2/\Omega_{ci}^2$ dependence [8]. We eliminate dependences upon $k_\perp/k_\parallel$ and $k_\perp^2 R_i^2$ by searching numerically for local maxima in the growth rate. Choosing $M/m = 1836$, we plot in Fig. 4 contours of maximum growth rate for

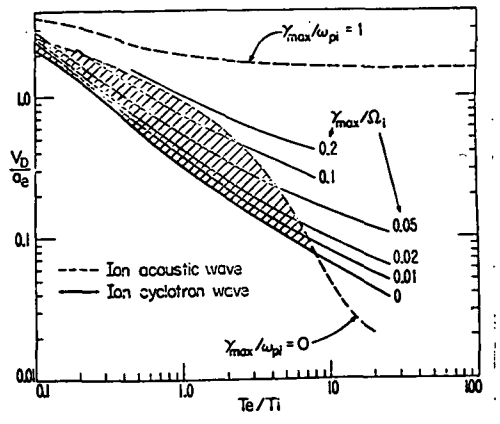

Fig. 4. Contours of maximum growth for the fundamental (n=1) ion cyclotron wave (solid) and ion acoustic wave (dashed).

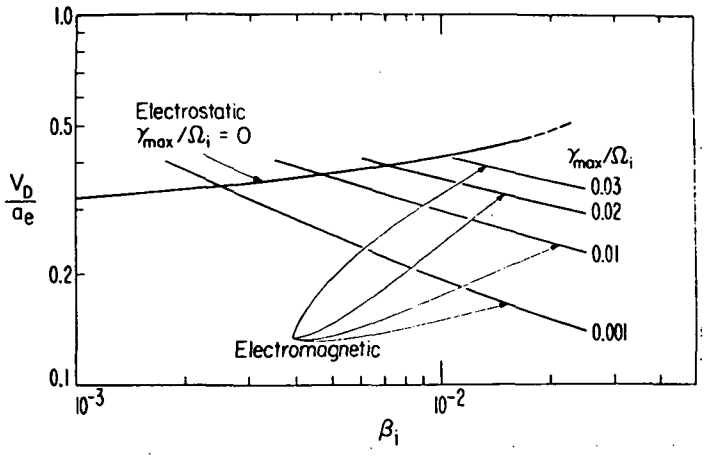

Fig. 5. Maximum growth rate contours for electromagnetic ion cyclotron waves and marginal stability boundary for electrostatic ion cyclotron waves.

the n = 1 wave as a function of the two remaining parameters, V_D/a_e and T_e/T_i; the marginal stability contour for the $k_\perp = 0$ ion acoustic wave, [7], [9]; and the contour for $\gamma_{max}/\omega_{pi} = 1$, the transition to the nonresonant electron-ion beam acoustic instability. The shaded region denotes where the ion cyclotron wave is unstable but the ion acoustic wave is stable. The ion cyclotron wave is unstable to a smaller current over the range $0.05 < T_e/T_i < 8.5$. Furthermore, it has a significant growth rate $\gamma_{max}/\Omega_i = 0.1$ (while the ion acoustic wave is still stable) over the range $0.25 < T_e/T_i < 2.5$. Some modes of Tokamak operation may fall in this range.

3.2 Electromagnetic Ion Cyclotron Waves.

The full electromagnetic wave dispersion relation for spatially hono-geneous, drifting electron and ion Maxwellian distributions in a uniform magnetic field has been solved. In addition to the parameters above, the dispersion relation now depends upon $\beta_i = 8\pi n T_i / B_0$. For β_i large enough, electromagnetic ion cyclotron waves have a parallel phase velocity sufficiently slow that they can be destabilized by small electron drifts [5]. Fig. 5 shows, for $M/m = 1836$ and $T_e/T_i = 1$, contours of constant maximum growth rate in a β_i, V_D/a_e parameter space, and the marginal stability contour $\gamma_{max}/\Omega_i = 0$, for the "electrostatic" ion cyclotron wave. This mode is electrostatically polarized for β_i small, and develops small electromagnetic components as β_i increases. Finite β_i corrections are stabilizing. However, the electromagnetic ion cyclotron wave has a lower threshold for $\beta_i > 10^{-3}$. For $\gamma_{max}/\Omega_i = 10^{-2}$, real $\omega \simeq 0.75\ \Omega_i$, and $k_\perp R_i \simeq 1.0 - 1.5$, $k_\parallel R_i < 0.1$. As V_D decreases to where $\gamma_{max}/\Omega_i < 10^{-3}$, $k_\perp R_i$ for maximum growth drops rapidly below 1.0 and $k_\parallel R_i$ increases.

3.3 Nonlinear Considerations

One-dimensional quasilinear electron plateau formation can saturate the electrostatic ion cyclotron instability at $e\phi/T_e \lesssim 10^{-2}$, ϕ = wave potential integrated over the unstable spectrum [4], [10]. Dum and Dupree [11], however, have shown that if electron plateau formation is inhibited, $e\phi/T_e \sim 1/2$, which agrees with Q machine results, [11], [12], [13], [14] where end effects may prevent plateau formation. We have observed [15] that resonance broadening due to large $e\phi/T_e$ permits ion cyclotron waves to interact with a significant portion of the electron distribution, leading to an effective electron-ion frequency $\nu_{eff} \simeq \sqrt{A}\Omega_{ci}(T_{e\parallel}/T_{i\perp})$ where A is the atomic number. In this limit, significant ion cyclotron anomalous resistance is possible.

Experiments in the Princeton Model ST may operate in regimes where the electrostatic ion cyclotron wave is unstable, but where the ion acoustic wave may not be unstable. [16], [17], [18] It has been suggested that larger β_i (higher density) may eliminate electrostatic current instabilities by reducing the electron drift needed to produce the confining magnetic field. However, we must still contend with the electromagnetic ion cyclotron instability. Bers, et al. [19] have suggested that ion cycltron waves may account for the perpendicular ion heating observed in the TM-3 Tokamak.

4. Turbulent Ion Heating

Ion acoustic turbulent heating of a cold ion beam injected into a plasma with initial $T_e/T_i \geq 10$ is observed in the UCLA DP (Double Plasma) device. A planar ion beam with drift energies exceeding T_e is accelerated from the driver plasma into the target plasma through a negatively biased grid. Fig. 6 shows the background and beam ion energy distribution functions [23] for various axial distances from the grid, as measured by an electrostatic energy analyzer [23]. For the $T_e = 1$ eV case, the beam attenuation is due to charge exchange. The apparent change of background density is largely instrumental and arises from the increase in the volume from which background ions may arrive at the analyzer as it is pulled away from the injection point. For $T_e = 1$ eV, and $T_i = 0.2$ eV, T_e/T_i is below marginal stability for the ion-ion beam instability [24] and the ion beam propagates with only a slight (if any)

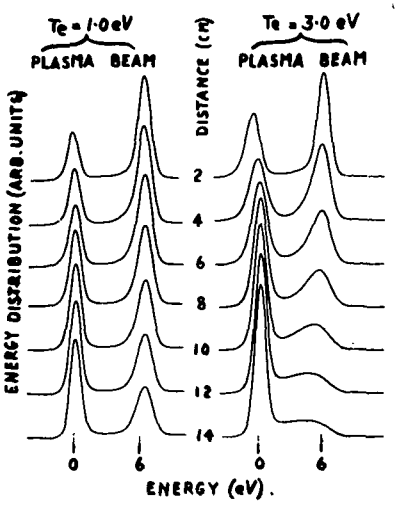

Fig. 6. Ion energy distribution vs. distance.

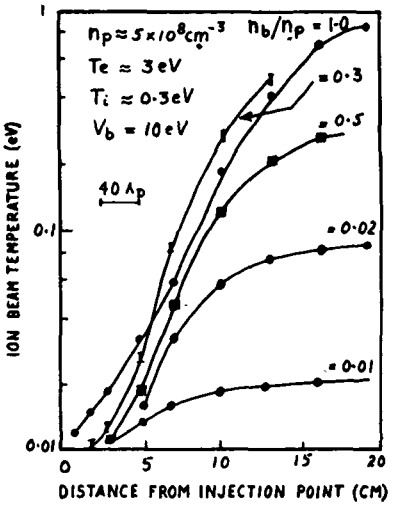

Fig. 7. Turbulent ion heating for various beam densities.

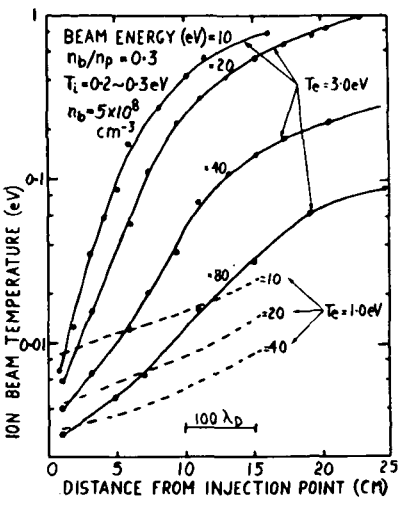

Fig. 8. Turbulent ion heating for various beam energies.

spreading in energy. For T_e = 3 eV, ion acoustic waves grow [2], and the ion beam broadens and eventually forms a quasi-linear type of plateau. Beam ions heat both parallel and perpendicular to the beam direction; background ions also heat.

In Fig. 7, the ion beam temperature vs. distance is displayed for several beam densities. The initial rate of ion temperature increase is approximately equal to the spatial linear growth rates of the ion acoustic waves. The dominant growing modes have wave numbers from 0.2 k_D to 0.6 k_D, and corresponding spatial growth rates of 0.01 k_D to 0.03 k_D. The ion acoustic waves saturate at a rms density fluctuation level of $\delta n/n_0$ 0.01 to 0.03. Ion heating continues after wave saturation, with the predominant beam kinetic to thermal energy transfer occurring in a distance $50\lambda_D$ to $100\lambda_D$ beyond the distance of maximum wave amplitude. In Fig. 8 the spatial growth of the beam temperature is displayed for various beam energies. The heating rates are reduced with increasing V_{beam}/c_s as expected from the decrease in the ion-ion instability growth rate with V_{beam}/c_s.

Directional probes show that when $V_{beam} > 2\ c_s$, waves grow obliquely to the beam, and that the wave energy densities parallel and perpendicular to the beam are comparable for dense beams. Second harmonics of the maximally unstable waves are also observed; since $k \simeq 0.5\ k_D$, these are probably generated by resonant mode couplings between oblique waves.

The initial exponential increase in ion beam temperature can be computed from quasi-linear theory. Taking the $(\underline{V} - \underline{V}_b)^2$ moment of the quasi-linear diffusion equation and assuming one dimensional, time independent conditions, we find that the beam temperature T_b satisfies

$$\partial T_b/\partial x = \frac{2}{N_b V_b} \sum_k N_k \gamma_k (\underline{k} \cdot \underline{V}_b - \omega) \qquad (4)$$

where $N_b V_b$ is the constant beam current, N_k is the wave action, and γ_k is the growth rate. N_k satisfies the approximate relation $V_g \partial N_k/\partial x \simeq 2\gamma_k N_k$. Substituting this into (4) and integrating, we find approximately

$$T_b(x) \simeq \frac{1}{N_b V_b} \sum_k V_g N_k(0)(\underline{k}\cdot\underline{V}_b - \omega) \exp[2k_i x] \qquad (5)$$

where $k_i = \gamma_k/V_g$ and only the x-dependence of N_k was considered.

To estimate the ion acoustic rms saturation amplitude $\delta n/n_0$, we utilize the results of strong turbulence theory (a la Dupree) by equating the initial linear growth rate γ to the effective turbulent collision frequency $\nu_{eff} = (k^2D)^{1/3} \simeq kc_s(\delta n/n_0)^{1/2}$ where D is the "average" velocity space diffusion coefficient. For $\gamma \sim k_i V_b$, and the observed $k_i/k \sim 1/20$ and $V_b/c_s \sim 2$, we find $\delta n/n_0 \sim 10^{-2}$. After turbulent wave saturation, the damping distance of the beam is $\Delta x \sim V_b/\nu_{eff} = V_b/kc_s(\delta n/n_0)^{-1/2}$. For the observed $k \sim 0.2\ k_D$ to $0.6\ k_D$, we then have $\Delta x \sim 30\lambda_D$ to $10^2\lambda_D$, in reasonable agreement with the experimental results; we conclude that the ion beam dissipation and thermalization are consistent with turbulent diffusion theories.

5. Collisionless Electrostatic Shocks

We have previously reported [21] data on steepening of ramp density waves, generated in DP devices, into collisionless electrostatic shocks ($n_1/n_0 \simeq 1.2$) where n_1 and n_0 are the densities behind and ahead of the shock. We report here extensions to turbulent and to larger amplitude shocks [22]. The turbulent transition regions are generated by the reflected ion beam. Either ambient ion fluctuations or injected ion waves can be amplified in the ion reflection region to give turbulence, an effect considerably enhanced by the addition of small amounts of a light ion species (Figs. 9 and 10).

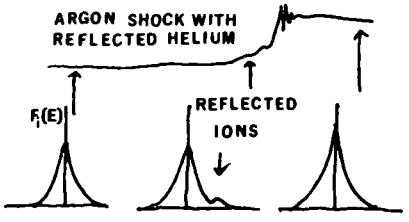

Fig. 9. Growth of natural ion acoustic turbulence in a helium/argon mixture ($n_{He}/n_A = 3\%$).

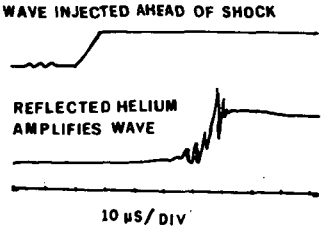

Fig. 10. Amplification of an injected wave train as it traverses the shock ($n_{He}/n_A = 3\%$).

When this occurs, the ion beam is scattered, resulting in a broadened distribution function.

The large amplitude shocks are generated by a photoionized slab ($n_R \simeq 10^9$) superimposed on a background of variable density, n_0. At a ratio R ($= n_R/n_0$) above 30, the slab expands freely, with no shock formation. Steep shocks begin to appear around R = 10, and propagate with density jumps $n_1/n_0 \simeq 2$. The jump decreases as R decreases, eventually overlapping our DP data when R = 1.5 and $n_1/n_0 \simeq 1.2$. Typical profiles are seen in Fig. 11. The trailing wave train, typical at Mach 1.1 to 1.2, is heavily damped at higher Mach numbers, e.g., 1.5. The trailing wave structure is also sensitive to T_e/T_i, essentially vanishing when T_e/T_i drops below 6. It is also very sensitive to the addition of light ions. Fig. 12 shows the effect of adding 3% helium to an argon plasma.

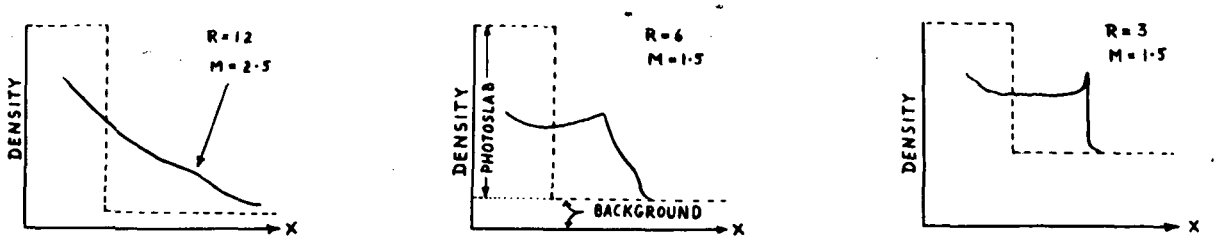

Fig. 11. Shock structure as a function of $R = n_R/n_0$.

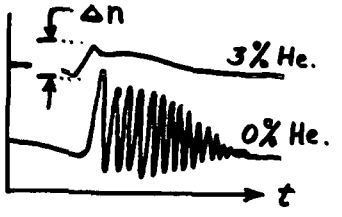

Fig. 12. Damping of trailing wave structure by light ions (He in A). $\Delta n/n \simeq 0.1$.

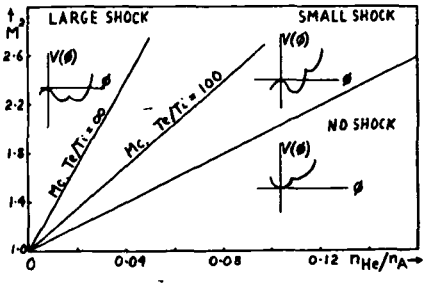

Fig. 13. Critical Mach number, M_c, for transition from small to large shocks, with $M \equiv V_{shock}/(T_e/M_A)^{1/2}$.

For a helium/argon mixture, we have studied the shock structure using cold fluid theory for the argon ions and a Vlasov treatment of the helium ions. The shock leading edge is simply described by the Sagdeev potential $V(\phi)$, [25] where $d^2\phi/dx^2 = -dV/d\phi$, ϕ = electrostatic potential. Above a critical Mach number, M_c, which depends on helium concentration and the ratio T_e/T_i as shown in Fig. 13, there exists a large amplitude shock which reflects almost all the helium ions and exhibits a double humped structure. Below the critical Mach number, $M < M_c$, most of the helium ions pass over the potential maximum which is thereby reduced approximately by the ratio m_{He}/m_A. (Below the lowest line, no shock exists in the He/A mixture.) This effect is present only if the helium ions are relatively cold ($T_e/T_{He} \gtrsim 20$).

REFERENCES

[1] SELLEN, J. M., BERNSTEIN, W., KEMP, R. F., Rev. Sci. Instr. 36 (1965) 316.

[2] IKEZI, H., TAYLOR, R. J., "Observation of Strong Ion-Acoustic Wave-Wave Interaction", UCLA Plasma Physics Group Report R-62 (1970).

[3] FIELD, E. C., FRIED, B. D., Phys. Fluids 7 (1964) 1937.

[4] DRUMMOND, W. E., ROSENBLUTH, M. N., Phys. Fluids 5 (1962) 1507.

[5] STIX, T. H., The Theory of Plasma Waves, McGraw-Hill, New York (1962) pp. 202 and 223.

[6] KINDEL, J. M., KENNEL, C. F., to appear, J. Geophys. Res. 76 (1971).

[7] STRINGER, T. E., J. Nucl. Energy, Pt. C, 6 (1965) 267.

[8] FORSLUND, D. W., KENNEL, C. F., KINDEL, J. M., Private Communication.

[9] FRIED, B. D., GOULD, R. W., Phys. Fluids 4 (1961) 139.

[10] PETVIASHVILI, V. I., Zh. Eksp. Teor. Fiz. 45 (1963) 1467 [Sov. Phys.-JETP 18 (1964) 1014].

[11] DUM, C. T., DUPREEE, T. H., Phys. Fluids 13 (1970) 2064.

[12] BOOTH, N., BAKER, D. R., STENZEL, R. L., WONG, A. Y., Bull. Am. Phys. Soc. 15 (1970) 1460; BOOTH, N., WONG, A. Y., UCLA Plasma Physics Group Report R-83, Jan. (1961).
[13] CHU, T. K., HENDEL, H. W., Private Communication.
[14] BUCHEL'NIKOVA, N. S., SALIMOV, R. A., Zh. Eksp. Teor. Fiz. 56 (1969) 1108 [Sov. Phys.-JETP 29 (1969) 595].
[15] KINDEL, J. M., KENNEL, C. F., Bull. Am. Phys. Soc. 15 (1970) 1460.
[16] GROVE, D. J., DIMOCK, D. L., HINNOV, E., HOSEA, J. C., JOHNSON, L. C., MESERVY, E. D., TOLNAS, E. L., Princeton Plasma Physics Laboratory (1970) MATT-813.
[17] PERKINS, F. W., RUTHERFORD, P. H., Private Communication.
[18] HIROSE, A., MURAKAMI, M., ALEXEFF, I., Oak Ridge National Laboratory Report (1970) ORNL-TM-2988.
[19] BERS, A., MANHEIMER, W., COPPI, B., Bull. Am. Phys. Soc. 15 (1970) 1419.
[20] FORSLUND, D. W., KENNEL, C. F., KINDEL, J. M., Bull. Am. Phys. Soc. 15 (1970) 1459.
[21] TAYLOR, R. J., BAKER, D., IKEZI, H., Phys. Rev. Letters 24 (1970) 206.
[22] MEANS, R., WONG, A. Y., Bull. Am. Phys. Soc. 15 (1970) 1409; UCLA Plasma Physics Group Report R-90, May (1971).
[23] IKEZI, H., TAYLOR, R. J., Phys. Rev. Letters 22 (1969) 923.
[24] FRIED, B. D., WONG, A. Y., Phys. Fluids 9 (1966) 1084.
[25] SAGDEEV, R. Z., MOISEEV, S. S., "Collisionless Shock Waves in a Plasma in a Weak Magnetic Field", Plasma Phys. (J. Nucl. Energy, Part C) 5 (1963) 43.